

Reliable Integer Ambiguity Resolution with Multi-Frequency Code Carrier Linear Combinations

Patrick Henkel¹ and Christoph Günther²

¹Technische Universität München, Germany

²German Aerospace Centre, Germany

Abstract

Carrier phase measurements are extremely accurate but ambiguous. The estimation of the integer ambiguities is in general split in two parts: A least-squares float solution, which is obtained by disregarding the integer property, and the actual fixing. The latter one can be a simple rounding, a sequential fixing (bootstrapping), or an integer least-squares estimation, which typically includes an integer decorrelation and a search. All these fixing methods suffer from a poor accuracy of the float solution due to the small carrier wavelengths. Moreover, the optimal integer least-squares estimation techniques are extremely sensitive to unknown biases.

This paper provides a new group of multi-frequency linear combinations to overcome the previous shortcomings: The combinations include both code and carrier phase measurements, and allow an arbitrary scaling of the geometry, an arbitrary scaling of the ionospheric delay, and any preferred wavelength. The maximization of the ambiguity discrimination results in combinations with a wavelength of several meters and a noise level of a few centimetres. These combinations are recommended for any application where reliability is more important than accuracy. This paper restricts to linear combinations for Galileo although the concept can be equally applied for GPS or any other GNSS system. Moreover, the paper provides an efficient method for the computation of the success rate of rounding.

Keywords: ambiguity resolution, multi-frequency code carrier linear combinations, pull-in regions, success rate

1. Introduction

Real-time kinematic (RTK) positioning uses double difference carrier phase measurements. The double differencing eliminates both receiver and satellite biases and clock offsets, which simplifies the resolution of the carrier phase integer ambiguities.

Currently, there exist mainly three error sources that limit the reliability of the integer resolution: First, there is the double difference ionospheric delay, which only cancels for short baselines. Secondly, the double difference tropospheric delay is often neglected, which introduces some errors especially if there is a significant difference in the height between both receivers. The third and probably most challenging error source is multipath. Fig. 1 shows the probability of wrong fixing for geometry-based widelane ambiguity resolution as a function of the baseline length. We can observe a substantial increase in the failure rate if there is an ionospheric gradient of 1 mm/km between both receivers. It causes a double difference ionospheric delay which occurs as a bias in the ambiguity resolution.

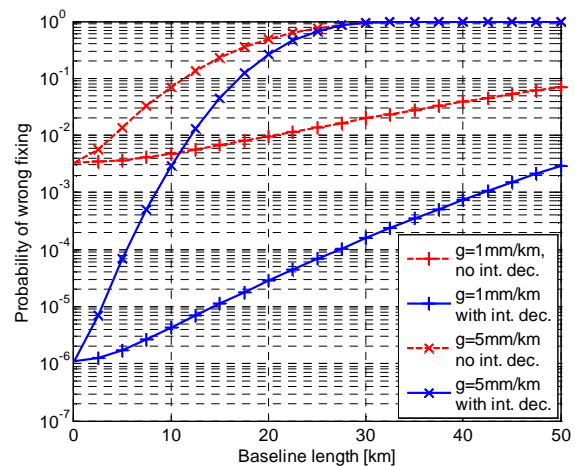


Figure 1: Reliability of geometry-based widelane ambiguity resolution with double difference Galileo measurements.

The probability of wrong fixings is shown in Fig. 1 for bootstrapping without and with integer decorrelation, whereas the latter one enables a certain improvement over the first one. Galileo double difference measurements on E1 and E5 were combined into an ionosphere-free code only combination and a phase-only combina-

tion with a wavelength of 78.2 cm. The latter combination amplifies the ionospheric delay by a factor 1.32. The failure rates significantly increase if the ionospheric gradient rises to 5 mm/km – a value which is still two orders of magnitude below the largest ionospheric gradient that has been observed so far. This is the motivation for the derivation and analysis of a new set of linear combinations that enable an arbitrary scaling of the ionospheric delay and any preferred wavelength.

2. Multi-Frequency Code Carrier Linear Combinations

Multi-frequency linear combinations are an efficient approach to improve the reliability of carrier phase integer ambiguity resolution. The linear combinations enable a significant suppression of the ionospheric delay and an increase in the wavelength, while the range information is kept. A systematic search of all possible dual frequency phase-only widelane combinations has been performed by Cocard and Geiger (1992) and by Collins (1999). An L1-L2 linear combination with a wavelength of 14.65 m was found. However, the combination also amplifies the ionospheric delay by more than 25 dB. The generalization to measurements on three and more frequencies enables much more attractive linear combinations as shown by Henkel and Günther (2007), by Wübena (2007), by Feng (2008), or by Richert and El-Sheimy (2007). For example, a Galileo triple frequency E1-E5a-E5b linear combination with a wavelength of 3.285 m suppresses the ionospheric delay by 17 dB. However, a complete elimination of the ionosphere is not achievable with phase-only widelane combinations.

Therefore, Henkel and Günther (2008) suggested the inclusion of code measurements in the linear combination. The ambiguity discrimination was introduced as an optimization criterion for the combinations: It was defined as the ratio between the wavelength and the doubled standard deviation of noise, and shall be maximized. The code measurements relax the integer constraint and enable the computation of a dual frequency geometry-preserving, ionosphere-free linear combination with a wavelength of 3.285 m and a noise level of a few centimetres. Henkel, Gomez and Günther (2009) computed multi-frequency code carrier linear combinations including the Galileo signals on E1, E5 and E6. Henkel (2009) gives a detailed derivation of code carrier combinations of maximum discrimination for an arbitrary number of frequencies. Three Carrier Ambiguity Resolution (TCAR) has been extensively analyzed also by Feng and Li (2009), Feng and Rizos (2009), Hatch (2006), and Hatch et al. (2000). They all considered linear combinations of carrier phase measurements to increase the combination wavelength, and linear combinations of code measurements to suppress the ionospheric delay. However, the degrees of freedom given by combining code

and carrier phases in a joint linear combination were not fully exploited, e.g. the code coefficients were restricted to integer numbers or the combination wavelength was derived only from the phase part of the combination.

In this section, the class of linear code carrier combinations is further generalized such that an arbitrary scaling of the geometry, an arbitrary scaling of the ionospheric delay, and any preferred wavelength are feasible. The code measurements from satellite k observed at user u on frequency m are modelled as

$$\begin{aligned} \rho_{u,m}^k &= \|\mathbf{x}_u - \mathbf{x}^k\| + (\mathbf{e}_u^k)^T \delta \mathbf{x}^k + c(\delta t_u - \delta t^k) \\ &+ T_u^k + q_{1m}^2 I_{u,1}^k + q_{1m}^3 I_{u,1}^k + b_{\rho_{u,m}} + b_{\rho_m^k} \\ &+ \ddot{o}_{\rho_{u,m}^k} + \varepsilon_{\rho_{u,m}^k}, \end{aligned} \quad (1)$$

with the user position \mathbf{x}_u , the satellite position \mathbf{x}^k , the unit vector \mathbf{e}_u^k pointing from the satellite to the receiver, the satellite position error $\delta \mathbf{x}^k$ due to imperfect knowledge of the orbit, the receiver clock offset δt_u , the satellite clock offset δt^k , the speed of light c , the tropospheric delay T_u^k , the ratio of frequencies $q_{1m} = f_1 / f_m$, the first and second order ionospheric delays $\{I_{u,1}^k, I_{u,1}^k\}$ on L1/E1, the receiver code bias $b_{\rho_{u,m}}$, the satellite code bias $b_{\rho_m^k}$, the delay $\ddot{o}_{\rho_{u,m}^k}$ due to code multipath, and the code noise $\varepsilon_{\rho_{u,m}^k}$. A similar model is used for the carrier phase measurements:

$$\begin{aligned} \lambda_m \varphi_{u,m}^k &= \|\mathbf{x}_u - \mathbf{x}^k\| + (\mathbf{e}_u^k)^T \delta \mathbf{x}^k + c(\delta t_u - \delta t^k) \\ &+ T_u^k - q_{1m}^2 I_{u,1}^k - \frac{1}{2} q_{1m}^3 I_{u,1}^k + b_{\varphi_{u,m}} + b_{\varphi_m^k} \\ &+ \ddot{o}_{\varphi_{u,m}^k} + \lambda_m N_{u,m}^k + \varepsilon_{\varphi_{u,m}^k}, \end{aligned} \quad (2)$$

with the wavelength λ_m and the carrier phase integer ambiguity $N_{u,m}^k$. The code and carrier phase measurements of (1) and (2) are linearly combined in (4) with the phase coefficient α_m and the code coefficient β_m . The choice of these coefficients is obtained from some constraints on the geometry, ionospheric delay, combined multipath and biases, and a further optimization that shall be described later in this section.

The first term on the right side of (4) describes the geometry term which can be scaled by any arbitrary value h_1 , i.e.

$$\sum_{m=1}^M (\alpha_m + \beta_m) = h_1. \quad (3)$$

$$\begin{aligned}
 \sum_{m=1}^M (\alpha_m \lambda_m \phi_{u,m}^k + \beta_m \rho_{u,m}^k) &= \left(\sum_{m=1}^M (\alpha_m + \beta_m) \right) \cdot \left(\|\mathbf{x}_u - \mathbf{x}^k\| + (\mathbf{e}_u^k)^T \delta \mathbf{x}^k + c(\delta \tau_u - \delta \tau^k) + T_u^k \right) - \left(\sum_{m=1}^M (\alpha_m - \beta_m) q_{1m}^2 \right) I_{u,1}^k \\
 &\quad - \left(\sum_{m=1}^M \left(\frac{1}{2} \alpha_m - \beta_m \right) q_{1m}^3 \right) I_{u,1}^k + \left(\sum_{m=1}^M \alpha_m \lambda_m N_{u,m}^k \right) + \left(\sum_{m=1}^M \alpha_m (b_{\phi_{u,m}^k} + b_{\phi_m^k}) + \beta_m (b_{\rho_{u,m}^k} + b_{\rho_m^k}) \right) \\
 &\quad + \left(\sum_{m=1}^M (\alpha_m \ddot{o}_{\phi_{u,m}^k} + \beta_m \ddot{o}_{\rho_{u,m}^k}) \right) + \left(\sum_{m=1}^M (\alpha_m \varepsilon_{\phi_{u,m}^k} + \beta_m \varepsilon_{\rho_{u,m}^k}) \right)
 \end{aligned} \tag{4}$$

A geometry-free combination is obtained if $h_1 = 0$ and a geometry-preserving one if $h_1 = 1$. Note that the scaling of the geometry also affects the orbital error, the clock offsets and the tropospheric delay. The first order ionospheric delay $I_{u,m}^k$ can also be scaled by any arbitrary value h_2 , i.e.

$$\sum_{m=1}^M (\alpha_m - \beta_m) q_{1m}^2 = h_2, \tag{5}$$

where $h_2 = 0$ corresponds to an ionosphere-free and $h_2 = -1$ to an ionosphere-preserving combination. However, a scaling factor in between -1 and 0 could be interesting if a certain ionospheric suppression is already achieved by double differencing. Similarly, the second order ionospheric delay can also be scaled by any value h_3 , i.e.

$$\left(\sum_{m=1}^M \left(\frac{1}{2} \alpha_m - \beta_m \right) q_{1m}^3 \right) = h_3, \tag{6}$$

The next term on the right side of (4) describes the linear combination of integer ambiguities, which shall be equal to a common wavelength λ times a single integer ambiguity N_u^k , i.e.

$$\sum_{m=1}^M \alpha_m \lambda_m N_{u,m}^k = \lambda N_u^k, \tag{7}$$

which can be easily solved for N_u^k :

$$N_u^k = \sum_{m=1}^M \underbrace{\frac{\alpha_m \lambda_m}{\lambda}}_{=j_m} N_{u,m}^k. \tag{8}$$

As $N_{u,m}^k$ is an unknown integer, j_m has to be integer valued to obtain an integer N_u^k . Rearranging (8) gives the phase coefficient

$$\alpha_m = \frac{j_m \lambda}{\lambda_m}, \tag{9}$$

which depends on the integer coefficient j_m and the combined wavelength λ . The next term on the right side of (4) includes the linear combination of code and carrier phase biases. It can also be considered in the combination design, e.g. by a pre-defined upper bound b_{\max} on the worst-case combination bias, i.e.

$$\sum_{m=1}^M \left(|\alpha_m| \cdot (|b_{\phi_{u,m}^k}| + |b_{\phi_m^k}|) + |\beta_m| \cdot (|b_{\rho_{u,m}^k}| + |b_{\rho_m^k}|) \right) \leq b_{\max}, \tag{10}$$

which requires some assumptions on the measurement biases. The superposition of multipath delays can also be included in the combination design, e.g. by

$$\sum_{m=1}^M \left(|\alpha_m| \cdot |\ddot{o}_{\phi_{u,m}^k}| + |\beta_m| \cdot |\ddot{o}_{\rho_{u,m}^k}| \right) \leq \ddot{o}_{\max}, \tag{11}$$

with some pre-defined upper bound \ddot{o}_{\max} on the worst-case superposition of multipath delays. These could be chosen from an elevation-dependant exponential function, i.e.

$$\ddot{o}_{\phi_{u,m}^k} = \ddot{o}_0 \cdot e^{-\frac{E}{\gamma}} \tag{12}$$

with the decay constant γ , elevation angle E and delay \ddot{o}_0 for $E = 0^\circ$. Finally, the last term on the right side of (4) describes the linear combination of phase and code noises. Its variance is given for statistically independent measurements by

$$(\sigma_u^k)^2 = \sum_{m=1}^M \left(\alpha_m^2 \sigma_{\phi_{u,m}^k}^2 + \beta_m^2 \sigma_{\rho_{u,m}^k}^2 \right), \tag{13}$$

and can be minimized under the consideration of all other constraints. Alternatively, the combinations can be optimized such that the reliability of ambiguity resolution is improved at the price of a slightly increased noise level. This motivated Henkel and Günther (2008) to

introduce the ambiguity discrimination as the ratio between the combination wavelength and the doubled noise standard deviation, i.e.

$$D = \frac{\lambda}{2\sigma}, \quad (14)$$

where the indices of the user and satellite were omitted to simplify notation. The ambiguity discrimination was further generalized by Henkel (2010b) to

$$D = \frac{\lambda}{\kappa_1\sigma + \kappa_2b}, \quad (15)$$

which includes a weighted sum of the combination noise and bias. The latter one can be neglected if ambiguity resolution is based on an ionosphere-free linear combination of double difference measurements, and if the multipath is sufficiently small. The maximization of the ambiguity discrimination corresponds to the minimization of the probability of wrong fixing for a geometry-free, ionosphere-free linear combination. As this paper is focussing more on the reliability than on the accuracy, the further analysis is restricted to the class of linear combinations that maximize D . Obviously, the maximization of the ambiguity discrimination makes the optimal combinations time-dependent, as the noise level typically depends on the satellite elevation. However, the optimal combinations do not change if the standard deviations of the code and phase measurements are scaled by a common factor on all frequencies. Note also that the optimization of the combinations can be easily performed in real-time.

Let us start the derivation (Henkel (2010a)) of optimum α_m and β_m by introducing the total phase coefficient

$$w_\phi = \sum_{m=1}^M \alpha_m = \lambda \sum_{m=1}^M \frac{j_m}{\lambda_m}, \quad (16)$$

which can be solved for the combination wavelength λ :

$$\lambda = \frac{w_\phi}{\sum_{m=1}^M \frac{j_m}{\lambda_m}}. \quad (17)$$

Replacing λ in (9) by (17) gives

$$\alpha_m = \frac{j_m}{\lambda_m} \lambda = \frac{j_m}{\lambda_m} \frac{1}{\sum_{m=1}^M \frac{j_m}{\lambda_m}} w_\phi. \quad (18)$$

The constraints on the geometry and first-order ionospheric delay are written in matrix-vector notation using (3), (5) and (18), i.e.

$$\Psi_1 \begin{bmatrix} \beta_1 \\ \beta_2 \end{bmatrix} + \Psi_2 \begin{bmatrix} w_\phi \\ \beta_3 \\ \vdots \\ \beta_M \end{bmatrix} = \begin{bmatrix} h_1 \\ h_2 \end{bmatrix}, \quad (19)$$

with

$$\Psi_1 = \begin{bmatrix} 1 & 1 \\ -1 & -q_{12}^2 \end{bmatrix} \quad (20)$$

and

$$\Psi_2 = \begin{bmatrix} 1 & 1 & \dots & 1 \\ \sum_{m=1}^M \frac{j_m}{\lambda_m} \frac{1}{\sum_{m=1}^M \frac{j_m}{\lambda_m}} q_{1m}^2 & -q_{13}^2 & \dots & -q_{1M}^2 \end{bmatrix}. \quad (21)$$

Note that the second order ionospheric delay has not been included in (19) as it is often negligible. Eq. (19) can be solved for the code coefficients β_1 and β_2 :

$$\begin{bmatrix} \beta_1 \\ \beta_2 \end{bmatrix} = \Psi_1^{-1} \left(\begin{bmatrix} h_1 \\ h_2 \end{bmatrix} - \Psi_2 \begin{bmatrix} w_\phi \\ \beta_3 \\ \vdots \\ \beta_M \end{bmatrix} \right) = \begin{bmatrix} s_1 + s_2 w_\phi + \sum_{m=3}^M s_m \beta_m \\ t_1 + t_2 w_\phi + \sum_{m=3}^M t_m \beta_m \end{bmatrix}, \quad (22)$$

where the s_m and t_m , $m \in \{1, \dots, M\}$, are implicitly defined by the last equality, i.e.

$$\begin{bmatrix} s_1 \\ t_1 \end{bmatrix} = \Psi_1^{-1} \begin{bmatrix} h_1 \\ h_2 \end{bmatrix} \quad (23)$$

$$\begin{bmatrix} s_2 \\ t_2 \end{bmatrix} = -\Psi_1^{-1} \Psi_2 \begin{bmatrix} 1 \\ 0^{M-2 \times 1} \end{bmatrix},$$

and

$$\begin{bmatrix} s_m \\ t_m \end{bmatrix} = -\Psi_1^{-1} \Psi_2 \begin{bmatrix} 0^{m-2 \times 1} \\ 1 \\ 0^{M-m \times 1} \end{bmatrix}. \quad (24)$$

Equation (22) leaves the integer coefficients j_m , $m \geq 1$, the code coefficients β_m , $m \geq 3$, and the total phase weight w_ϕ as unknowns. The maximization of D over these variables shall be performed in two steps as shown in Fig. 2.

$$D(\mathbf{w}_\phi, \boldsymbol{\beta}) = \sum_{m=1}^M \frac{j_m}{\lambda_m} \frac{1}{\kappa_1 \boldsymbol{\sigma} + \kappa_2 \mathbf{b}} \quad \text{with} \quad \begin{cases} \boldsymbol{\sigma} = \sqrt{\tilde{\eta}^2 \mathbf{w}_\phi^2 + (s_1 + s_2 \mathbf{w}_\phi + \mathbf{s}^T \boldsymbol{\beta})^2 \sigma_{\rho_1}^2 + (t_1 + t_2 \mathbf{w}_\phi + \mathbf{t}^T \boldsymbol{\beta})^2 \sigma_{\rho_2}^2 + \boldsymbol{\beta}^T \boldsymbol{\Sigma} \boldsymbol{\beta}} \\ \mathbf{b} = \mathbf{w}_\phi \cdot |\mathbf{b}_\phi| + |s_1 + s_2 \mathbf{w}_\phi + \mathbf{s}^T \boldsymbol{\beta}| \cdot |\mathbf{b}_{\rho_1}| + |t_1 + t_2 \mathbf{w}_\phi + \mathbf{t}^T \boldsymbol{\beta}| \cdot |\mathbf{b}_{\rho_2}| + (\mathbf{d}(\boldsymbol{\beta}))^T \boldsymbol{\beta} \end{cases} \quad (25)$$

$$\kappa_1 \cdot \left(\sum_{m=1}^M \frac{j_m}{\lambda_m} \frac{(s_1 + s_2 \mathbf{w}_\phi + \mathbf{s}^T \boldsymbol{\beta}) \mathbf{s} \cdot \sigma_{\rho_1}^2 + (t_1 + t_2 \mathbf{w}_\phi + \mathbf{t}^T \boldsymbol{\beta}) \mathbf{t} \cdot \sigma_{\rho_2}^2 + \boldsymbol{\beta}^T \boldsymbol{\Sigma} \boldsymbol{\beta}}{\sqrt{\tilde{\eta}^2 \mathbf{w}_\phi^2 + (s_1 + s_2 \mathbf{w}_\phi + \mathbf{s}^T \boldsymbol{\beta})^2 \sigma_{\rho_1}^2 + (t_1 + t_2 \mathbf{w}_\phi + \mathbf{t}^T \boldsymbol{\beta})^2 \sigma_{\rho_2}^2 + \boldsymbol{\beta}^T \boldsymbol{\Sigma} \boldsymbol{\beta}}} \right) \quad (26)$$

$$+ \kappa_2 \cdot (\text{sgn}(s_1 + s_2 \mathbf{w}_\phi + \mathbf{s}^T \boldsymbol{\beta}) \mathbf{s} \cdot |\mathbf{b}_{\rho_1}| + \text{sgn}(t_1 + t_2 \mathbf{w}_\phi + \mathbf{t}^T \boldsymbol{\beta}) \mathbf{t} \cdot |\mathbf{b}_{\rho_2}| + \mathbf{d}(\boldsymbol{\beta})) \stackrel{!}{=} 0$$

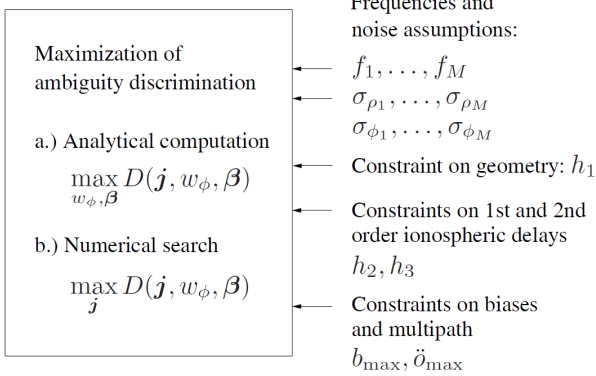


Figure 2: Computation of multi-frequency code carrier linear combinations of maximum discrimination

First, a numerical search is performed with a maximization over j_m and, secondly, an analytical computation is performed with a maximization over \mathbf{w}_ϕ and $\boldsymbol{\beta}_m$. Equation (25) provides an expression of the ambiguity discrimination that is obtained from (15) using (17), (18), (22) and (13), and only depends on \mathbf{w}_ϕ and $\boldsymbol{\beta}$. Some abbreviations were introduced to simplify the notation:

$$\tilde{\eta}^2 = \sum_{m=1}^M \frac{j_m^2}{\lambda_m^2} \frac{1}{\left(\sum_{m=1}^M \frac{j_m}{\lambda_m} \right)^2} \sigma_{\phi_m}^2, \quad (27)$$

$$\boldsymbol{\Sigma} = \begin{bmatrix} \sigma_{\rho_3}^2 & \cdots & \sigma_{\rho_3 \rho_M} \\ \vdots & \ddots & \vdots \\ \sigma_{\rho_3 \rho_M} & \cdots & \sigma_{\rho_M}^2 \end{bmatrix}, \quad (28)$$

$$\mathbf{d}(\boldsymbol{\beta}) = \begin{bmatrix} \text{sgn}(\beta_3) \cdot |\mathbf{b}_{\rho_3}| \\ \vdots \\ \text{sgn}(\beta_M) \cdot |\mathbf{b}_{\rho_M}| \end{bmatrix} \quad (29)$$

as well as $\boldsymbol{\beta} = [\beta_3, \dots, \beta_M]^T$, $\mathbf{s} = [s_3, \dots, s_M]^T$ and $\mathbf{t} = [t_3, \dots, t_M]^T$.

The maximization of D with respect to \mathbf{w}_ϕ results in the constraint

$$\frac{\partial D}{\partial \mathbf{w}_\phi} \stackrel{!}{=} 0, \quad (30)$$

and the maximization with respect to $\boldsymbol{\beta}$ gives

$$\frac{\partial D}{\partial \boldsymbol{\beta}} \stackrel{!}{=} 0. \quad (31)$$

The latter constraint is developed in (26), which results in a highly nonlinear relationship between \mathbf{w}_ϕ and $\boldsymbol{\beta}$ that can be solved only numerically. Therefore, the further analysis shall be restricted to $\kappa_1 = 2$ and $\kappa_2 = 0$.

In this case, (26) can be substantially simplified using $(\mathbf{x}^T \mathbf{y}) \mathbf{z} = (\mathbf{x}^T \mathbf{z}) \mathbf{y}$, i.e.

$$\begin{aligned} & (s_1 + s_2 \mathbf{w}_\phi + \mathbf{s}^T \boldsymbol{\beta}) \mathbf{s} \cdot \sigma_{\rho_1}^2 \\ & + (t_1 + t_2 \mathbf{w}_\phi + \mathbf{t}^T \boldsymbol{\beta}) \mathbf{t} \cdot \sigma_{\rho_2}^2 + \boldsymbol{\beta}^T \boldsymbol{\Sigma} \boldsymbol{\beta} \\ & = \underbrace{[\sigma_{\rho_1}^2 \mathbf{s} \mathbf{s}^T + \sigma_{\rho_2}^2 \mathbf{t} \mathbf{t}^T + \boldsymbol{\Sigma}]}_{\mathbf{A}} \boldsymbol{\beta} \\ & + \underbrace{[s_2 \sigma_{\rho_1}^2 \mathbf{s} + t_2 \sigma_{\rho_2}^2 \mathbf{t}]}_{\mathbf{b}} \mathbf{w}_\phi + \underbrace{[s_1 \sigma_{\rho_1}^2 \mathbf{s} + t_1 \sigma_{\rho_2}^2 \mathbf{t}]}_{\mathbf{c}} = \mathbf{0}, \end{aligned} \quad (32)$$

which shows a linear relationship between \mathbf{w}_ϕ and $\boldsymbol{\beta}$. Solving (32) for $\boldsymbol{\beta}$ yields

$$\boldsymbol{\beta} = -\mathbf{A}^{-1}(\mathbf{c} + \mathbf{b} \cdot \mathbf{w}_\phi). \quad (33)$$

The first constraint in (30) can be further developed as

$$\begin{aligned} & (s_1 + s_2 w_\phi + \mathbf{s}^T \boldsymbol{\beta})(s_1 + \mathbf{s}^T \boldsymbol{\beta}) \cdot \sigma_{\rho_1}^2 \\ & + (t_1 + t_2 w_\phi + \mathbf{t}^T \boldsymbol{\beta})(t_1 + \mathbf{t}^T \boldsymbol{\beta}) \cdot \sigma_{\rho_2}^2 + \boldsymbol{\beta}^T \boldsymbol{\Sigma} \boldsymbol{\beta} = 0, \end{aligned} \quad (34)$$

and replacing $\boldsymbol{\beta}$ by (33) gives

$$\begin{aligned} & (s_1 + s_2 w_\phi - \mathbf{s}^T \mathbf{A}^{-1}(\mathbf{c} + \mathbf{b} w_\phi)) \cdot (s_1 - \mathbf{s}^T \mathbf{A}^{-1}(\mathbf{c} + \mathbf{b} w_\phi)) \cdot \sigma_{\rho_1}^2 \\ & + (t_1 + t_2 w_\phi - \mathbf{t}^T \mathbf{A}^{-1}(\mathbf{c} + \mathbf{b} w_\phi)) \cdot (t_1 - \mathbf{t}^T \mathbf{A}^{-1}(\mathbf{c} + \mathbf{b} w_\phi)) \cdot \sigma_{\rho_2}^2 \\ & + (\mathbf{c} + \mathbf{b} w_\phi)^T (\mathbf{A}^{-1})^T \boldsymbol{\Sigma} \mathbf{A}^{-1} (\mathbf{c} + \mathbf{b} w_\phi) = 0, \end{aligned} \quad (35)$$

which only includes w_ϕ (and \mathbf{j}_m , hidden in $\mathbf{A}, \mathbf{b}, \mathbf{c}, \mathbf{s}$ and \mathbf{t}) as unknowns. Equation (35) is a quadratic equation in w_ϕ , i.e.

$$r_0 + r_1 \cdot w_\phi + r_1^2 \cdot w_\phi^2 = 0, \quad (36)$$

with

$$\begin{aligned} r_0 &= (s_1 - \mathbf{s}^T \mathbf{A}^{-1} \mathbf{c})^2 \sigma_{\rho_1}^2 + (t_1 - \mathbf{t}^T \mathbf{A}^{-1} \mathbf{c})^2 \sigma_{\rho_2}^2 \\ &+ \left(\mathbf{c}^T (\mathbf{A}^{-1})^T \boldsymbol{\Sigma} \mathbf{A}^{-1} \mathbf{c} \right) \\ r_1 &= \left((s_1 - \mathbf{s}^T \mathbf{A}^{-1} \mathbf{c})(-\mathbf{s}^T \mathbf{A}^{-1} \mathbf{b}) \right. \\ &+ (s_2 - \mathbf{s}^T \mathbf{A}^{-1} \mathbf{b})(s_1 - \mathbf{s}^T \mathbf{A}^{-1} \mathbf{c}) \left. \right) \cdot \sigma_{\rho_1}^2 \\ &+ \left((t_1 - \mathbf{t}^T \mathbf{A}^{-1} \mathbf{c})(-\mathbf{t}^T \mathbf{A}^{-1} \mathbf{b}) \right. \\ &+ (t_2 - \mathbf{t}^T \mathbf{A}^{-1} \mathbf{b})(t_1 - \mathbf{t}^T \mathbf{A}^{-1} \mathbf{c}) \left. \right) \cdot \sigma_{\rho_2}^2 \\ &+ \left(\mathbf{c}^T (\mathbf{A}^{-1})^T \boldsymbol{\Sigma} \mathbf{A}^{-1} \mathbf{b} + \mathbf{b}^T (\mathbf{A}^{-1})^T \boldsymbol{\Sigma} \mathbf{A}^{-1} \mathbf{c} \right) \\ r_2 &= (s_2 - \mathbf{s}^T \mathbf{A}^{-1} \mathbf{b})(-\mathbf{s}^T \mathbf{A}^{-1} \mathbf{b}) \cdot \sigma_{\rho_1}^2 \\ &+ (t_2 - \mathbf{t}^T \mathbf{A}^{-1} \mathbf{b})(-\mathbf{t}^T \mathbf{A}^{-1} \mathbf{b}) \cdot \sigma_{\rho_2}^2 \\ &+ \mathbf{b}^T (\mathbf{A}^{-1})^T \boldsymbol{\Sigma} \mathbf{A}^{-1} \mathbf{b}. \end{aligned} \quad (37)$$

The latter term r_2 always vanishes which can be proven by replacing $\mathbf{A}, \mathbf{b}, \mathbf{c}, \mathbf{s}$ and \mathbf{t} by their definitions. Thus, the optimal total phase coefficient is given by

$$w_{\phi_{\text{opt}}} = -\frac{r_0}{r_1}. \quad (38)$$

The optimal phase and code coefficients α_m and β_m are then obtained from (33), (22) and (18). The α_m and β_m can be optimized for any standard deviation σ_{ρ_m} . In this paper, the σ_{ρ_m} are chosen according to the Cramer Rao bound, which is given by

$$\sigma_{\rho_m} \geq \Gamma_m = \sqrt{\frac{c^2}{\frac{C}{N_0} T_i \cdot \frac{\int (2\pi f)^2 |S_m(f)|^2 df}{\int |S_m(f)|^2 df}}}, \quad (39)$$

with the speed of light c , the carrier to noise power ratio C/N_0 , the pre-detection integration time T_i , and the power spectral density $S_m(f)$. The latter one has been derived by Betz (2002) for binary offset carrier (BOC) modulated signals.

Tab. 1 shows the Cramer Rao bounds of the wideband Galileo signals, which are used in the further analysis. For GPS, stochastic models for the code and carrier phase measurements including its time correlation have been extensively analyzed during the last years, e.g. by Wang et al. (1998), Bona (2000), Tiberius and Kenselaar (2000) and Li et al. (2008). The obtained standard deviations are larger than those given in Tab. 1 due to the smaller signal bandwidths and different modulation (BPSK instead of BOC) of GPS.

Table 1: Cramer Rao bounds for Galileo signals at $C/N_0 = 45$ dB-Hz and $T_i = 1s$

Signal	BW [MHz]	Γ [cm]	
E1	MBOC	20	11.14
E5	AltBOC(15,10)	51	1.95
E5a	BPSK(10)	20	7.83
E5b	BPSK(10)	20	7.83
E6	BPSK(5)	20	11.36

Tab. 2, 3 and 4 show the optimized dual, triple and four frequency code carrier widelane combinations of maximum discrimination for $\sigma_\phi = 1\text{mm}$ and $\sigma_{\rho_m} = \Gamma_m$.

The first line in each table represents a geometry-preserving (GP) ionosphere-free (IF) combination, followed by a GP reduced ionosphere (IR, 10 dB suppression) combination that can be used for differential positioning over medium length baselines. The next linear combination is a geometry-free (GF), ionosphere-preserving (IP) one, which could be applied for the estimation of the ionospheric delay. The last combination is both GF and IF, which makes it a candidate for ambiguity resolution, or multipath analysis. A scaled version of this combination was recently used by Li et al. (2010).

The linear combinations are characterized by a wavelength of a few meters and a noise level of several centimeters, which results in a large ambiguity discrimination D . The GP-IF combination tends to a slightly larger D than the GF-IP one but both discriminations are large enough to enable a reliable integer ambiguity resolution if multipath and biases can be estimated. A comparison of Tab. 2 and Tab. 3 shows that the processing of the E5 signal as a single wideband signal is preferred over the processing of two subbands, i.e. the lower code noise of the AltBOC signal more than compensates for the slightly reduced number of degrees of freedom. The inclusion of E6 measurements further increases the ambiguity discrimination, which achieves its highest value for the E5a-E5b wideband ambiguity combination. Note

also that all code coefficients β_m of the triple and four frequency GF-IF combinations are quite small, which indicates a large robustness over code multipath.

The search of the optimal integer coefficients j_m was performed over $|j_m| \leq 4$ to avoid large noise amplification, and further constrained by $\sigma < 0.4\text{m}$ to prevent combinations of extremely large wavelengths, that also result in a large noise level. The wavelength of the GF, IF linear combination was set to 1 m as this type of combinations leave one degree of freedom: The discrimination is independent of λ and both the GF and IF constraints are fulfilled for any λ .

Table 2: Dual-frequency code carrier wideband combinations of maximum discrimination for $\sigma_\phi = 1\text{mm}$ and $\sigma_p = \Gamma_m$

h_1	h_2	E1		E5		λ	σ	D
1	0	j_1	1	j_2	-1	3.285 m	6.5 cm	25.12
		α_1	17.2629	α_2	-13.0593			
		β_1	-0.0552	β_2	-3.1484			
1	-0.1	j_1	1	j_2	-1	3.092 m	6.1 cm	25.55
		α_1	16.2508	α_2	-12.2936			
		β_1	-0.0487	β_2	-2.9085			
0	-1	j_1	-1	j_2	1	1.938 m	4.9 cm	19.65
		α_1	-10.1831	α_2	7.7035			
		β_1	0.0737	β_2	2.4059			
0	0	j_1	-1	j_2	1	1 m	8.2 cm	6.09
		α_1	-5.2550	α_2	3.9754			
		β_1	0.7285	β_2	0.5511			
h_1	h_2	E1		E5a		λ	σ	D
1	0	j_1	1	j_2	-1	4.309 m	31.4 cm	6.87
		α_1	22.6467	α_2	-16.9115			
		β_1	-1.0227	β_2	-3.7125			

Table 3: Triple-frequency code carrier wideband combinations of maximum discrimination for $\sigma_\phi = 1\text{mm}$ and $\sigma_p = \Gamma_m$

h_1	h_2	E1		E5b		E5a		λ	σ	D
1	0	j_1	1	j_2	-4	j_3	3	3.603 m	13.9 cm	12.99
		α_1	18.9326	α_2	-58.0271	α_3	42.4139			
		β_1	-0.2871	β_2	-0.9899	β_3	-1.0423			
1	-0.1	j_1	1	j_2	-4	j_3	3	3.368 m	12.7 cm	13.26
		α_1	17.6991	α_2	-54.2465	α_3	39.6505			
		β_1	-0.2499	β_2	-0.9013	β_3	-0.9519			
0	-1	j_1	1	j_2	-4	j_3	3	2.543 m	12.3 cm	9.98
		α_1	-12.8901	α_2	39.5074	α_3	-28.8772			
		β_1	0.4477	β_2	0.9061	β_3	0.9061			
0	0	j_1	0	j_2	-1	j_3	1	1 m	0.8 cm	62.71
		α_1	0	α_2	-4.0266	α_3	3.9242			
		β_1	0.0004	β_2	0.0480	β_3	0.0540			

Table 4: Four-frequency code carrier widelane combinations of maximum discrimination for $\sigma_\phi = 1\text{mm}$ and $\sigma_\rho = \Gamma_m$

h_1	h_2	E1		E6		E5b		E5a		λ	σ	D
1	0	j_1	1	j_2	-3	j_3	0	j_4	2	3.998 m	6.5 cm	31.02
		α_1	21.0108	α_2	-51.1627	α_3	0	α_4	31.3798			
		β_1	-0.0239	β_2	-0.0349	β_3	-0.0824	β_4	-0.0867			
1	-0.1	j_1	1	j_2	-3	j_3	0	j_4	2	3.753 m	6.0 cm	31.22
		α_1	19.7197	α_2	-48.0187	α_3	0	α_4	29.4514			
		β_1	-0.0154	β_2	-0.0233	β_3	-0.0554	β_4	-0.0585			
0	-1	j_1	-1	j_2	4	j_3	-1	j_4	-2	2.505 m	5.1 cm	24.81
		α_1	-13.1658	α_2	42.7460	α_3	-10.0881	α_4	-19.6632			
		β_1	0.0285	β_2	0.0274	β_3	0.0576	β_4	0.0576			
0	0	j_1	0	j_2	0	j_3	-1	j_4	1	1 m	0.8 cm	64.27
		α_1	0	α_2	0	α_3	-4.0266	α_4	3.9242			
		β_1	-0.0038	β_2	0.0140	β_3	0.0429	β_4	0.0493			

3. Reliable Integer Ambiguity Resolution

In this section, the linear combinations of the previous section are used for reliable integer ambiguity resolution. The following model is used for the code and carrier phase measurements from all visible satellites:

$$\Psi = \mathbf{H}\xi + \mathbf{A}\mathbf{N} + \eta, \quad (40)$$

where \mathbf{H} denotes the geometry matrix, ξ includes all unknown real-valued parameters, \mathbf{A} is the wavelength matrix, \mathbf{N} are the integer ambiguities, and $\eta \sim N(\mathbf{0}, \Sigma)$

is the white Gaussian measurement noise. Note that Ψ can either consist of uncombined code and carrier phase measurements (traditional approach), or of two optimized GP linear combinations (our approach): a code carrier combination of maximum discrimination and a code-only combination of minimum noise amplification. In both cases, the estimation of ξ can be separated from the integer ambiguity resolution by an orthogonal projection, i.e.

$$\mathbf{P}_H^\perp \Psi = \underbrace{\mathbf{P}_H^\perp \mathbf{A}}_{\tilde{\mathbf{A}}} \mathbf{N} + \mathbf{P}_H^\perp \eta, \quad (41)$$

with $\mathbf{P}_H^\perp = \mathbf{1} - \mathbf{H}(\mathbf{H}^T \Sigma^{-1} \mathbf{H})^{-1} \mathbf{H}^T \Sigma^{-1}$. The least-squares float ambiguity solution follows from (41) as

$$\hat{\mathbf{N}} = (\tilde{\mathbf{A}}^T \Sigma^{-1} \tilde{\mathbf{A}})^{-1} \tilde{\mathbf{A}}^T \Sigma^{-1} \Psi \quad (42)$$

with the covariance

$$\Sigma_{\hat{\mathbf{N}}} = (\tilde{\mathbf{A}}^T \Sigma^{-1} \tilde{\mathbf{A}})^{-1}. \quad (43)$$

The most simple integer estimation technique is rounding of the float solution of (42). The success rate heavily depends on the conditioning of the equation system. It is

characterized by the condition number which is defined as the ratio between the largest and smallest eigenvalue of $\Sigma_{\hat{\mathbf{N}}}$.

The success rate can be increased by a sequential integer estimation which also takes the correlation between the float estimates into account. It was introduced by Blewitt (1989) and is given by

$$\hat{N}_{k|1,\dots,k-1} = \hat{N}_k - \sum_{j=1}^{k-1} \sigma_{\hat{N}_k \hat{N}_{j|1,\dots,j-1}} \sigma_{\hat{N}_{j|1,\dots,j-1}}^{-2} \cdot (\hat{N}_{j|1,\dots,j-1} - [\hat{N}_{j|1,\dots,j-1}]) \quad (44)$$

with the conditional variance $\sigma_{\hat{N}_{k|1,\dots,k-1}}^2$ and the covariance

$\sigma_{\hat{N}_k \hat{N}_{j|1,\dots,j-1}}$. As the conditional ambiguity estimates are uncorrelated, the success rate of sequential ambiguity fixing can be efficiently computed from the product of one-dimensional cumulative Gaussian distributions, i.e.

$$P_s = \prod_{k=1}^K \left(\int_{-0.5}^{+0.5} \frac{1}{\sqrt{2\pi\sigma_{\hat{N}_{k|1,\dots,k-1}}^2}} \cdot e^{-\frac{(\epsilon_{\hat{N}_{k|1,\dots,k-1}} - b_{\hat{N}_{k|1,\dots,k-1}})^2}{2\sigma_{\hat{N}_{k|1,\dots,k-1}}^2}} d\epsilon_{\hat{N}_{k|1,\dots,k-1}} \right) \quad (45)$$

Teunissen (1999) showed that bootstrapping as well as any other integer ambiguity resolution technique can be fully described by so called pull-in regions. A pull-in region represents the set of all float ambiguities $\hat{\mathbf{N}}$ that are mapped to the same integer vector $\tilde{\mathbf{N}}_k$. The map $S_{\tilde{\mathbf{N}}_k}$ is given by

$$S_{\tilde{\mathbf{N}}_k} = \left\{ \hat{\mathbf{N}} \in \mathbb{R}^{K \times 1} \mid \tilde{\mathbf{N}}_k = S(\hat{\mathbf{N}}) \right\}, \quad \tilde{\mathbf{N}}_k \in \mathbb{Z}^{K \times 1} \quad (46)$$

These pull-in regions shall now be analysed for the optimal integer least-squares estimation of widelane ambiguities, i.e.

$$\hat{\mathbf{N}} = \arg \min_{\mathbf{N}} \left\| \hat{\mathbf{N}} - \mathbf{N} \right\|_{\Sigma_{\hat{\mathbf{N}}}}^2. \quad (47)$$

Fig. 3 shows these regions for a double difference carrier phase positioning over a large baseline with a good satellite geometry. Subfigure (a) refers to the estimation of the E1 integers and subfigure (b) to the widelane ambiguities.

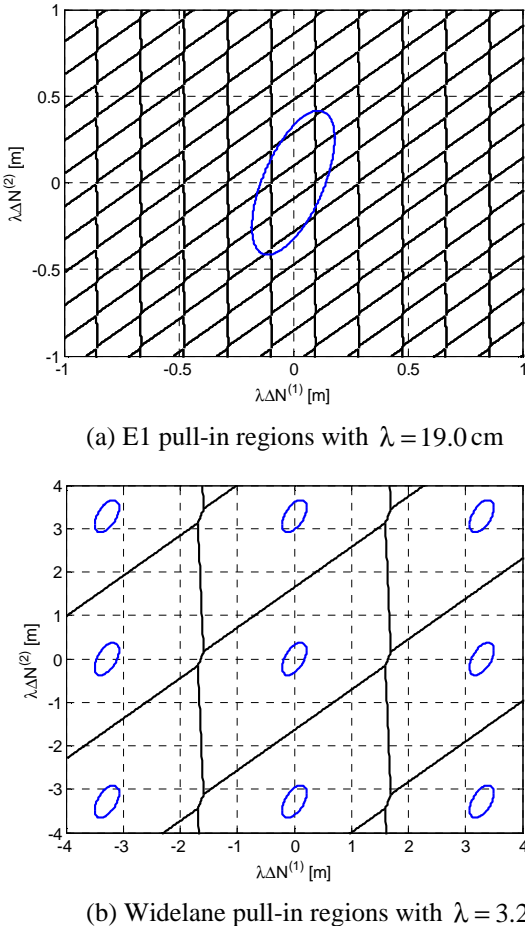


Figure 3: Increase of pull-in regions with multi-frequency linear combinations for Galileo

Obviously, the increase in the wavelength from 19.0 cm to 3.285 m substantially increases the size of the pull-in regions. Both figures also include the error ellipse given by $\left\| \hat{\mathbf{N}} - \mathbf{N} \right\|_{\Sigma_{\hat{\mathbf{N}}}}^2 = c$ with $c = 3$. Its size is larger than the size of the pull-in region for uncombined ambiguities but significantly smaller than the size of the widelane pull-in regions. This is another indication for extremely reliable ambiguity resolution with our linear combinations. The integer least-squares estimation can be efficiently performed with the Least-squares Ambiguity Decorrelation Adjustment (LAMBDA) method of Teunissen (1995). The size of the error ellipse in Fig. 3 is typical for a long-

baseline kinematic positioning with a good satellite geometry and measurements from only a few epochs.

Fig. 4 shows the benefit of geometry-preserving ($h_1 = 1$), ionosphere-free ($h_2 = 0$) linear combinations for Wide-Area Real-Time Kinematics (WA-RTK). If no linear combinations are used, the baseline (once per epoch), the integer ambiguities (using bootstrapping with integer decorrelation), the tropospheric wet zenith delay and its rate, the ionospheric slant delays for all satellites and their rates have to be estimated from double difference measurements on at least two frequencies. Here, the wideband Galileo signals on E1 (CBOC modulation) and E5 (AltBOC modulated) were considered at a carrier to noise power ratio of 45 dB-Hz.

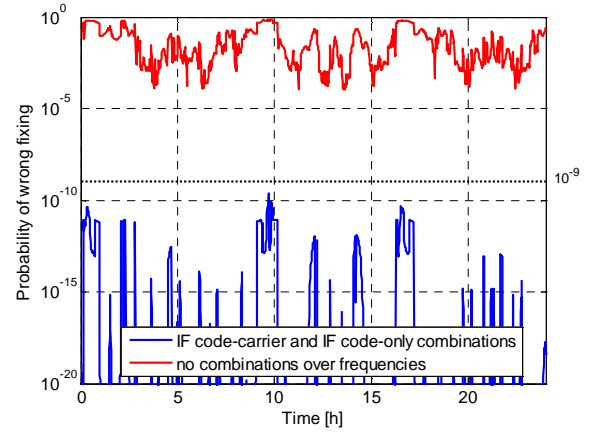


Figure 4: Benefit of E1-E5 mixed code carrier linear combinations for reliable integer ambiguity resolution

The small wavelength and the large number of unknown parameters result in a rather poor probability of wrong fixing, which varies between 10^{-4} and 1 depending on the satellite geometry. This is far too much for Safety-of-Life critical applications where a failure rate of at most 10^{-9} is required. Therefore, the use of an optimized multi-frequency code carrier combination of maximum discrimination and of a code-only combination of minimum noise amplification is analysed. As both linear combinations are ionosphere-free, the latter two parameter sets do not have to be estimated. Fig. 4 shows that the probability of wrong fixing can be reduced by several orders of magnitude due to the large wavelength of 3.285 m. The 10^{-9} requirement is fulfilled for any satellite geometry.

Fig. 5 shows the benefit of a different class of linear combinations: the geometry-free ($h_1 = 0$) ones, which eliminate also the clock offsets, orbital errors and tropospheric delay.

The benefit is analysed for differential positioning with triple frequency (E1, E5a, E5b) receiver-receiver single difference 1 Hz measurements of 20 s.

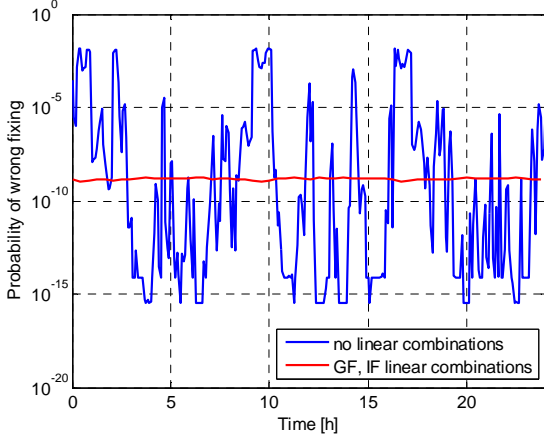


Figure 5: Benefit of geometry-free, ionosphere-free linear combinations for integer ambiguity resolution

If no linear combinations are used, the carrier phase integer ambiguities, the baseline (once/ epoch), the differential receiver clock offset (once/ epoch), the ionospheric slant delays and their rates, as well as the tropospheric wet zenith delay and its rate have to be estimated. In this traditional approach, the ambiguities were resolved sequentially according to (44) with integer decorrelation based on uncombined measurements. The use of linear combinations significantly simplifies the ambiguity resolution: It directly provides an integer estimate that only has to be averaged over T epochs, i.e.

$$\hat{N}^k = \frac{1}{T} \sum_{t=1}^T \left(\frac{1}{\lambda} \sum_{m=1}^M (\alpha_m \lambda_m \phi_m^k(t) + \beta_m \rho_m^k(t)) \right) \quad (48)$$

$$\sim N(N^k + b_u^k, \sigma_{\hat{N}^k}^2),$$

with

$$\sigma_{\hat{N}^k} = \frac{\sigma}{\lambda \sqrt{T}} = \frac{1}{2D\sqrt{T}}, \quad (49)$$

and thus justifies the maximization of the ambiguity discrimination D . As geometry-free linear combinations imply an independent fixing of the ambiguities from all satellites, the probability of wrong fixing can be efficiently computed from

$$P_s = \prod_{k=1}^K \int_{-0.5}^{+0.5} \frac{1}{\sqrt{2\pi\sigma_{\hat{N}_k}^2}} \cdot e^{-\frac{(\epsilon_{\hat{N}_k} - b_{N_k})^2}{2\sigma_{\hat{N}_k}^2}} d\epsilon_{\hat{N}_k} \quad (50)$$

Fig. 5 shows that this probability of wrong fixing is almost constant over time and enables a substantial improvement over the traditional approach especially for poor satellite geometries. In this case, the benefit due to the increase in λ from 19 cm to 1 m more than compensates for the degradation due to individual satellite processing.

4. Success rate determination for rounding of float solution

Simple rounding of the float solution has recently received little attention mainly for two reasons: First, it provides a lower success rate than sequential bootstrapping and integer least-squares estimation for unbiased measurements. Secondly, there does not exist a closed-form expression for the evaluation of the success rate of rounding. Therefore, the easily computable success rate of bootstrapping became the de-facto standard, either used as a lower bound for integer least-squares estimation or directly used to characterize bootstrapping.

However, the simple rounding could be an interesting candidate for precise point positioning as it is less sensitive with respect to unknown biases than sequential ambiguity fixing and integer least-squares estimation. The sequential estimation accumulates the biases of various satellites, which could either cancel or amplify. In a worst-case scenario, the integer decorrelation further amplifies them, and the search might additionally reduce the success rate due to the negligence of biases. The simple rounding prevents all these disadvantages. Consequently, there is a need for an efficient computation of the success rate of rounding as Monte-Carlo simulations are practically unacceptable for error rates in the order of magnitude of 10^{-9} . Genz (1992) suggested an efficient method for the evaluation of the multivariate cumulative normal distribution. This method uses three integral transformations and shall be applied for the evaluation of the success rate which is given by

$$P_s = P([\hat{N}] = N) = \frac{1}{\sqrt{|\Sigma_{\hat{N}}|} (2\pi)^K}$$

$$= \int_{-0.5-b_1}^{+0.5-b_1} \dots \int_{-0.5-b_K}^{+0.5-b_K} e^{-\frac{1}{2} \epsilon_{\hat{N}}^T \Sigma_{\hat{N}}^{-1} \epsilon_{\hat{N}}} d\epsilon_{\hat{N}_1} \dots d\epsilon_{\hat{N}_K}, \quad (51)$$

where $\epsilon_{\hat{N}} = \hat{N} - N$ denotes the error of the float solution \hat{N} . It is normal distributed, i.e.

$$\epsilon_{\hat{N}} \sim N(\mathbf{0}, \Sigma_{\hat{N}}), \quad (52)$$

with the float ambiguity covariance matrix $\Sigma_{\hat{N}}$.

The Cholesky decomposition is used to diagonalize the error vector, i.e.

$$\mathbf{e}_{\hat{N}} = \mathbf{C}^{-1} \boldsymbol{\varepsilon}_{\hat{N}}, \quad (53)$$

with

$$\boldsymbol{\Sigma}_{\hat{N}} = \mathbf{C}\mathbf{C}^T. \quad (54)$$

Thus, the success rate of (51) can be rewritten as

$$\begin{aligned} P_s = & \frac{1}{\sqrt{(2\pi)^K}} \int_{l_1}^{u_1} e^{-\frac{e_{\hat{N}_1}^2}{2}} \int_{l_2(e_{\hat{N}_1})}^{u_2(e_{\hat{N}_1})} e^{-\frac{e_{\hat{N}_2}^2}{2}} \dots \\ & \cdot \int_{l_k(e_{\hat{N}_1, \dots, e_{\hat{N}_{k-1}}})}^{u_k(e_{\hat{N}_1, \dots, e_{\hat{N}_{k-1}}})} e^{-\frac{e_{\hat{N}_k}^2}{2}} de_{\hat{N}_1} de_{\hat{N}_2} \dots de_{\hat{N}_k}, \end{aligned} \quad (55)$$

where the correlation between the float ambiguities is included in the integration limits l_k and u_k . These limits are obtained from the inequalities

$$-0.5 - b_k \leq \varepsilon_{\hat{N}_k} = \sum_{j=1}^k C_{kj} e_{\hat{N}_j} \leq +0.5 - b_k, \quad (56)$$

which can be solved for $e_{\hat{N}_k}$:

$$l_k \leq e_{\hat{N}_k} \leq u_k \quad (57)$$

with

$$\begin{aligned} l_k &= \frac{-0.5 - b_k - \sum_{j=1}^{k-1} C_{kj} e_{\hat{N}_j}}{C_{kk}} \\ u_k &= \frac{+0.5 - b_k - \sum_{j=1}^{k-1} C_{kj} e_{\hat{N}_j}}{C_{kk}}. \end{aligned} \quad (58)$$

The second transformation uses the cumulative normal distribution to absorb the exponential functions of (55):

$$z_k = \Phi(e_{\hat{N}_k}), \quad (59)$$

with

$$\Phi(v) = \frac{1}{\sqrt{2\pi}} \int_{-\infty}^v e^{-\frac{\theta^2}{2}} d\theta. \quad (60)$$

Thus, (53) simplifies to

$$P_s = \int_{l_1}^{u_1} \int_{l_2(z_1)}^{u_2(z_1)} \dots \int_{l_k(z_1, \dots, z_{k-1})}^{u_k(z_1, \dots, z_{k-1})} dz_1 dz_2 \dots dz_k, \quad (61)$$

with the transformed integration limits

$$\begin{aligned} l'_k &= \Phi\left(\frac{1}{C_{kk}} \left(-0.5 - b_k - \sum_{j=1}^{k-1} C_{kj} \Phi^{-1}(z_j)\right)\right) \\ u'_k &= \Phi\left(\frac{1}{C_{kk}} \left(+0.5 - b_k - \sum_{j=1}^{k-1} C_{kj} \Phi^{-1}(z_j)\right)\right). \end{aligned} \quad (62)$$

Finally, Genz's third transformation is given by

$$w_k = \frac{z_k - l'_k}{u'_k - l'_k}, \quad (63)$$

which puts the integral into a constant limit form, i.e.

$$\begin{aligned} P_s = & (u'_1 - l'_1) \int_0^1 (u'_2 - l'_2) \int_0^1 \dots \\ & (u'_k - l'_k) \int_0^1 dw_1 dw_2 \dots dw_k, \end{aligned} \quad (64)$$

Eq. (64) can be expanded to

$$\begin{aligned} P_s = & (u'_1 - l'_1) \int_0^1 (u'_2 - l'_2) f(w_1) \int_0^1 \dots \\ & (u'_k - l'_k) f(w_{k-1}) \int_0^1 f(w_k) dw_1 dw_2 \dots dw_k, \end{aligned} \quad (65)$$

with

$$f(w_k) = \begin{cases} 1 & \text{if } 0 \leq w_k \leq 1 \\ 0 & \text{else.} \end{cases} \quad (66)$$

The introduction of $f(w_k)$ does not change the value of P_s but it allows to interpret w_k as a uniformly distributed random variable between 0 and 1. Thus, (65) can also be written as

$$P_s = E_{w_1, \dots, w_k} \left\{ \prod_{k=1}^K (u'_k(w_1, \dots, w_k) - l'_k(w_1, \dots, w_k)) \right\}, \quad (67)$$

with $w_k \sim U(0,1)$ for all k .

The success rate of (67) can be efficiently computed using Monte-Carlo simulation.

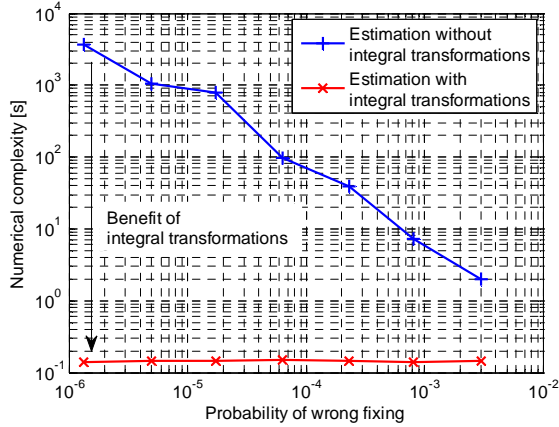


Figure 6: Efficient computation of success rate of rounding with integral transformations.

Genz (1992) suggests the subregion adaptive method to further improve the efficiency of the numerical integration. Fig. 6 shows the benefit of computing the expectation value w.r.t. w_k in (67) instead of w.r.t. ϵ_N in (51). The computational burden is measured by the time required to estimate P_s with a dual core 2.1 GHz CPU. The use of the three integral transformations enables a substantial reduction in the computation time. A real-time evaluation becomes also feasible.

Fig. 7 shows the probability of wrong fixing for various integer estimation techniques. An ionosphere-free carrier smoothing is applied to two GP-IF linear combinations (a code carrier combination of maximum discrimination and a code-only combination) of E1 and E5 measurements to improve the reliability of widelane ambiguity resolution. Obviously, a larger smoothing period results in a lower error rate. For unbiased measurements, the integer least-squares estimation achieves the lowest error rate of all fixing methods.

A slightly higher error rate can be observed for sequential fixing with integer decorrelation due to the lack of an integer search. An additional degradation occurs if the integer decorrelation is omitted, and the largest error rate is obtained for rounding as it does not consider the correlations between the float ambiguity estimates. The ranking of the fixing techniques completely changes in the presence of biases. An elevation dependent exponential bias profile was chosen to analyze the impact of multipath. A worst-case accumulation over all visible satellites is considered as described by Henkel et al. (2009). The magnitude of the code multipath was set to 1 cm for a satellite in the zenith and to 10 cm for a satellite in the horizon. For the phase multipath, 0.01 cycles and 0.1

cycles were assumed respectively. In this case, rounding achieves the lowest error rate, followed by sequential fixing without and with integer decorrelation. The integer decorrelation amplifies the biases and the search criterion is suboptimal which results in the largest error rate. Consequently, the simplest method is also the most robust one: the rounding of the float solution.

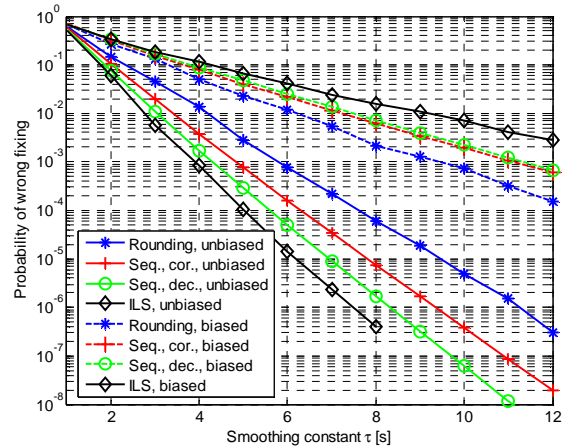


Figure 7: Comparison of various integer ambiguity resolution techniques for both unbiased and biased measurements with worst-case accumulation of biases.

5. Conclusion

In this paper, a new group of linear combinations was analyzed that include both code and carrier phase measurements on two or more frequencies. An arbitrary scaling of the geometry, an arbitrary scaling of the ionospheric delay, and any preferred wavelength can be obtained with these linear combinations. The maximization of the ambiguity discrimination leads to combinations with a wavelength of several meters and a noise level of a few centimetres. The integer ambiguities of these combinations can be resolved with a probability of wrong fixing of less than 10^{-9} with measurements from a few epochs. These combinations are recommended for any application where reliability is more important than accuracy.

Moreover, an efficient method for the computation of the success rate of rounding of the float solution is suggested. It is based on a transformation of the cumulative multivariate Gaussian distribution into uniform distributions, which can be efficiently evaluated in real-time. The rounding of the float solution was considered for two reasons: First, the linear combinations improve the conditioning of the equation system such that there is no strong need of an integer decorrelation. Secondly, rounding of the float solution is much less sensitive with respect to multipath and biases than bootstrapping and integer least-squares estimation. Both the optimized

multi-frequency linear combinations with large wavelengths and the efficient computation of the success rate are seen as two steps to improve the reliability of ambiguity resolution for precise point positioning.

References

- Betz J. (2002), **Binary Offset Carrier Modulations for Radionavigation**, Navigation, Vol. 48, No. 4, pp. 227-246.
- Bona P., (2000), **Precision, cross correlation, and time correlation of GPS phase and code observations**, GPS Sol., Vol. 4, No. 2, pp. 3-13.
- Blewitt G., (1989), **Carrier phase ambiguity resolution for the Global Positioning System applied to geodetic baselines up to 2000 km**, J. of Geophys. Res., Vol. 94, No. B8, pp. 10.187-10.302.
- Cocard M. and A. Geiger (1992), **Systematic search for all possible widelanes**, Proc. of 6-th Int. Geod. Symp. on Sat. Pos., Ohio, USA, pp. 312-318.
- Collins P. (1999), **An overview of GPS inter-frequency carrier phase combinations**, Techn. Memor., Geodetic Survey Division, University of New Brunswick, Canada, pp. 1-15.
- Feng Y. (2008), **GNSS three carrier ambiguity resolution using ionosphere-reduced virtual signals**, J. of Geodesy, Vol. 82, No. 12, pp. 847-862.
- Feng Y. and B. Li (2009), **Three Carrier Ambiguity Resolutions: Generalized Problems, Models and Solutions**, J. of Global Positioning Systems, Vol. 8, No. 2, pp. 116-124.
- Feng Y. and C. Rizos (2009), **Network-based geometry-free three carrier ambiguity resolution and phase bias calibration**, GPS Sol., Vol.13, No. 1, pp. 43-56.
- Genz A. (1992), **Numerical Computation of Multivariate Normal Probabilities**, J. of Comp. and Graph. Stat., pp. 141-149.
- Hatch R. (2006), **A new three-frequency, geometry-free technique for ambiguity resolution**, Proc. of ION GNSS, Fort Worth, USA, pp. 309-316.
- Hatch R., J. Jung, P. Enge and B. Pervan (2000), **Civilian GPS: The benefits of three frequencies**, GPS Sol., Vol. 3, No. 4, pp. 1-9.
- Henkel P. (2009), **Bootstrapping with Multi-Frequency Mixed Code Carrier Linear Combinations and Partial Integer Decorrelation in the Presence of Biases**, Proc. of Int. Assoc. of Geod. (IAG) Scient. Ass., Buenos Aires, Argentina.
- Henkel P. (2010a), **Reliable Integer Ambiguity Resolution with Multi-Frequency Code Carrier Linear Combinations**, Proc. of 23rd Int. Techn. Meet. of the Inst. of Nav. (ION-GNSS), Portland, USA.
- Henkel P. (2010b), **Reliable Carrier Phase Positioning**, Verlag Dr. Hut, Technische Universität München, 177 pp.
- Henkel P., V. Gomez and C. Günther (2009), **Modified LAMBDA for absolute carrier phase positioning in the presence of biases**, Proc. of the Int. Techn. Meet. of the Inst. of Nav. (ION-ITM), San Diego, USA, pp. 642-651.
- Henkel P. and C. Günther (2007), **Three frequency linear combinations for Galileo**, Proc. of 4-th IEEE Workshop on Pos., Nav. and Comm. (WPNC), Hannover, Germany, pp. 239-245.
- Henkel P. and C. Günther (2008), **Joint L-/C-Band Code and Carrier Phase Linear Combinations for Galileo**, Int. J. of Nav. and Obs., Vol. 2008, Article ID 651437, 8 pp.
- Li B., Y. Feng and Y. Shen (2010), **Three carrier ambiguity resolution: distance-independent performance demonstrated using semi-generated triple frequency GPS signals**, GPS Sol., Vol. 14, pp. 177-184.
- Li B., Y. Shen and P. Xu (2008), **Assessment of stochastic models for GPS measurements with different types of receivers**, Chin. Sci. Bul., Vol. 53, No. 20, pp. 3219-3225.
- Richert T. and N. El-Sheimy (2007), **Optimal linear combinations of triple frequency carrier phase data from future global navigation satellite systems**, GPS Solut., Vol. 11, pp. 11-19.
- Tiberius C. and F. Kenselaar (2000), **Estimation of the stochastic model for GPS code and phase observation**, Surv. Rev., Vol. 35, No. 277, pp. 441-454.
- Teunissen P. (1995), **The least-squares ambiguity decorrelation adjustment: a method for fast GPS ambiguity estimation**, J. of Geodesy, Vol. 70, pp. 65-82.
- Teunissen P. (1999), **An optimality property of the integer least-squares estimator**, J. of Geodesy, Vol. 73, pp. 587-593.

Wang J., M. Stewart and M. Sakiri (1998), **Stochastic modelling for static GPS baseline data processing**, *J. Surv. Eng.*, Vol. 124, No. 4, pp. 171-181.

Wübbena G. (2007), **New GNSS Signals and Ambiguity Resolution**, Proc. of EGU Gen. Ass., Vienna, Austria.

Biography

Patrick Henkel studied electrical engineering and information technology at the Technische Universität München, Munich, Germany, and the Ecole Polytechnique de Montréal, Montréal, Canada. He received his diploma in 2005. He then started his PhD on reliable carrier phase positioning at the Technische Universität München and graduated with summa cum laude in 2010. He is now working towards his habilitation in the field of precise point positioning. He visited the Mathematical Geodesy and Positioning group at TU Delft as a guest researcher in 2007, and the GPS Lab at Stanford University in 2008 and 2010. He received the Pierre Contensou Gold Medal at the International Astronautical Congress in 2007, the Bavarian regional prize at the European Satellite Navigation Competition in 2010, and the Vodafone Förderpreis for his dissertation in 2011. He is one of the founders of AMCONAV GmbH, which develops differential carrier phase receiver systems.